Supporting Information for:

Evaluating the Native Oxide of Titanium as an Electrocatalyst for Oxalic Acid Reduction

*Halilu Sale[1,2], Zeliha Ertekin[1,3], Paula L. Lalaguna[1], Malcolm Kadodwala[1], Mark D. Symes[1]**

1. School of Chemistry, University of Glasgow, G12 8QQ Glasgow, UK.
2. Energy Commission of Nigeria, Plot 701c Garki-Abuja, Nigeria
3. Hacettepe University, Faculty of Science, Department of Chemistry, Beytepe, 06800 Ankara, Turkey.

Corresponding author email: mark.symes@glasgow.ac.uk

Materials and Chemicals

The following materials were obtained from their respective suppliers and used without further purification: oxalic acid (anhydrous for synthesis, Sigma-Aldrich, 99.0%), sulfuric acid (H_2SO_4, Fisher Chemical, 95.0%), acetone (technical grade, VWR chemicals, ≥ 99.0%), sodium sulfate (Na_2SO_4, Sigma-Aldrich, 99.0%), argon (Ar, supplied by BOC, 99.99%), titanium foil (Thermo-Scientific, 0.25mm thick, 99.5% metal basis), platinum foil (Pt, Alfa Aesar, 0.25 mm, 99.99% metals basis), Nafion membrane (Nafion-117, manufactured by Fuel Cell Store).

Preparation of Electrodes

The titanium foil obtained from Thermo-Scientific and was mechanically cut into 1 × 1 cm pieces (2 cm^2 total area, including both the front and back of the electrode) for cyclic voltammetry or 2 × 1 cm (4.0 cm^2 total area) pieces for bulk electrolysis experiments. Thereafter, the electrodes were ultrasonically cleaned in deionised water with a resistance of 15 MΩ for 5 minutes each to clean the surfaces; the cleaned titanium electrodes were then dried under air and were used as cathode materials. Platinum foil was used as the anode.

Bulk Electrolysis methods

Bulk electrolysis was performed by chronoamperometry; 40 mL of 0.03 M oxalic acid in 0.2 M Na_2SO_4 solution (pH = 2.2) was used in the cathodic compartment. The solution's pH was measured with a pH meter (Hanna Instruments, HI 9025). In the anodic compartment, a solution of 0.2 M Na_2SO_4 (pH = 7.1) was employed, and the pH of the anodic compartment was adjusted by adding 1 M H_2SO_4 dropwise until it reached the same pH as the cathodic compartment. Bulk electrolysis was conducted using Gamry potentiostat/galvanostat (Gamry Instruments Interface 1010E) for two hours at each potential, over the range −0.5 to −0.7 V (vs RHE) at a temperature of 25 °C. The bulk electrolysis setup is depicted in Figure S1.

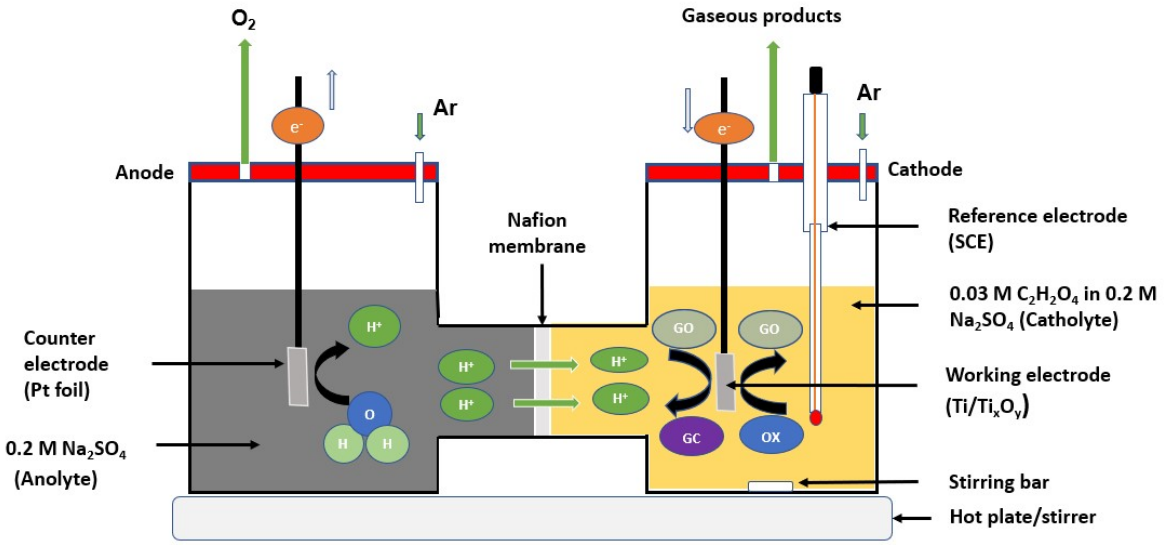

Figure S1: The H-cell set-up used for the electrochemical reduction of oxalic acid (OX) to glyoxylic acid (GO) and glycolic acid (GC). The right-hand compartment of the cell is where the working electrode (Ti foil with a surface area of 4 cm^2) and a reference electrode (SCE) were placed, while the left-hand side contains the anolyte where the counter electrode (platinum foil) was placed. The two compartments were separated by a Nafion membrane. The experiment was conducted at a temperature of 25 °C for 2 hours at each applied potential.

Electrode Characterisation methods

X-ray photoelectron spectroscopy (XPS) was performed using a Scienta 300 with SPECS monochromated X-Ray Source (Al Kα source, photon energy 1486.6 eV operating at approximately 12 kV and 200 W) at St Andrews University. Thin film X-ray diffraction (XRD) analysis was performed using Rigaku Mini Flex with Cu Kα radiation. The scanning diffraction angle 2θ range was collected from 5 to 90° at a scan speed of 5° per min. Ellipsometry and atomic force microscopy were performed to evaluate the thickness and roughness/smoothness of the native oxides, respectively. Ellipsometry was performed using a variable-angle ellipsometer (M-2000XI Ellipsometer, J. A. Woollam) to measure the amplitude and phase changes in the wavelength range 210-1690 nm at different angles of incidence, while atomic force microscopy (AFM) was performed using a Dimension Icon Atomic Force Microscope System with ScanAsyst using a silicon tip (ScanAsyst-Air-HPI) and peak force tapping. A scan size of 10 mm, a scan rate of 0.3 Hz and 512 samples/line were used for all the measurements. The surface roughness was obtained using Gwyddion software. The electrochemical active surface area (ECSA) was determined through the cyclic

voltammetry technique.[3,4] Electrochemical impedance spectroscopy (EIS) measurements were conducted using a Gamry potentiostat/galvanostat (Gamry Instruments Interface 1010E) using three electrode settings ranging from 1×10^5 to 1×10^{-1} Hz. A constant polarisation potential (−0.6 V *vs* RHE) was applied during EIS measurements. The equivalent circuit model parameters were determined using Gamry Echem Analyst software.

HPLC Analysis

The liquid products were analysed by Agilent high-performance liquid chromatography (HPLC) using an Aminex HPX-87H, 300 mm × 7.8 mm column. The mobile phase used was 0.1% formic acid in acetonitrile (HPLC grade) and 0.1% formic acid in water in a ratio of 30:70, respectively. The HPLC machine was set at a flow rate of 0.6 mL/min, at a temperature of 60 °C, and a detector wavelength of 210 - 230 nm was used. The chromatogram and the retention time for the respective products are represented in Figure S2.

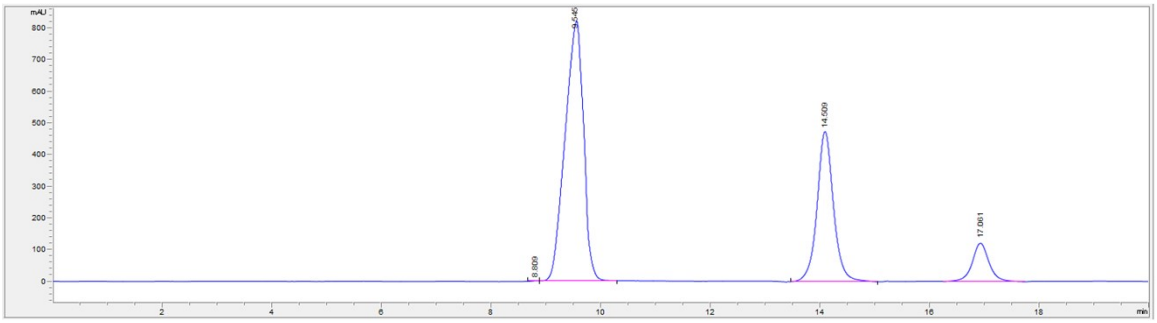

Figure S2: HPLC chromatogram for electrochemical reduction of oxalic acid to glyoxylic acid and glycolic acid at an applied potential of −0.6 V vs RHE at 25 °C.

Faradaic efficiencies

Based on the molar concentration of the oxalic acid used as the starting material for the reduction process, the following equations (S1 - S4)[1] are used to evaluate the performance of the electrode (Ti/Ti_xO_y) in reducing oxalic acid, and the results are presented in Table S1.

$$FE\ (\%) = \frac{m_{product} \times n\ \times F}{Q} \times 100 \qquad (Equation\ S1)$$

Where *FE* = Faradaic efficiency, $m_{product}$ = moles of the reduction products, *n* = number of electrons needed for the formation of the products from oxalic acid (n = 2 and 4 for the formation of glyoxylic and glycolic acid, respectively), *F* = Faraday's constant (96485 C mol^{-1}) and Q = total charge in coulombs passed over the duration of the electrolysis.

The percentage conversion of oxalic acid in the experiment was computed thus:

$$Conversion\ (\%) = \frac{[OX]_i - [OX]_t}{[OX]_i} \times 100 \quad (Equation\ S2)$$

Where, $[OX]_i$ = the initial concentration of oxalic acid, and $[OX]_t$ = the concentration of oxalic acid at the end of the electrolysis.

The yield (Y) of the respective products was calculated as follows:

$$Yield\ to\ m_{[GO]}\ (\%) = \frac{[GO]_t}{[OX]_i} \times 100 \qquad (Equation\ S3)$$

$$Yield\ to\ m_{[GC]}\ (\%) = \frac{[GC]_t}{[OX]_i} \times 100 \qquad (Equation\ S4)$$

Where, $[GO]_t$ = the concentration of $m_{[GO]}$ after 2 h of reaction time, $[GC]_t$ = the concentration of $m_{[GC]}$ after 2 h of reaction time; [*OX*], [*GO*] and [*GC*] are the molar concentrations of oxalic, glyoxylic, and glycolic acids, respectively.

Table S1: The average Faradaic efficiency, oxalic acid conversion, percentage yields and current densities for electrochemical reduction of oxalic acid on titanium electrodes for 2 hours at 25 °C.

Potentials (V vs RHE)	Faraday efficiency (%)		Oxalic Acid Conversion (%)	Yield (%)		Current Density (mA/cm^2)
	Glyoxylic acid	Glycolic acid		Glyoxylic acid	Glycolic acid	
−0.5	47.0	38.0	31.0	20.5	8.3	−3.5
−0.6	43.0	32.8	38.4	27.3	10.5	−5.1
−0.7	23.6	19.2	34.2	22.3	9.1	−7.6

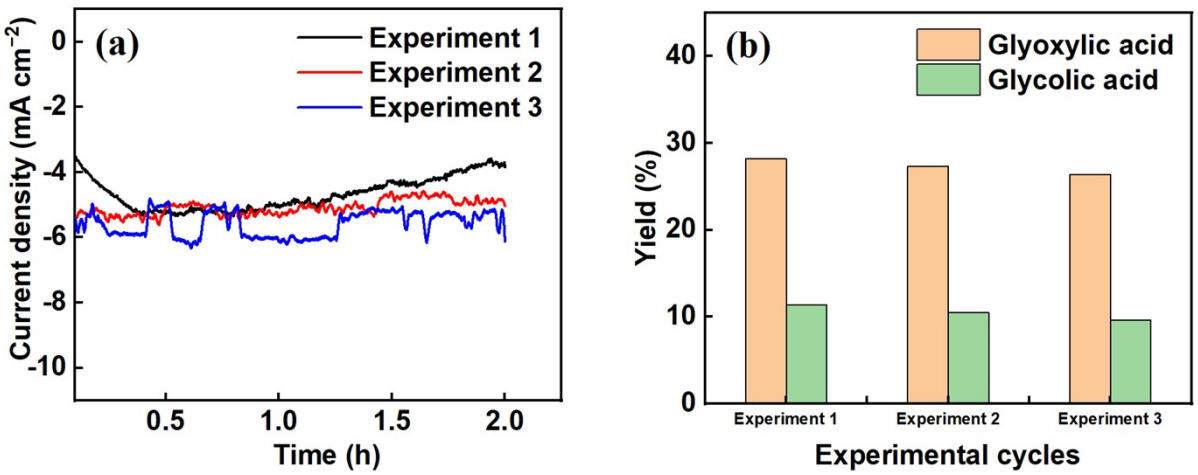

Figure S3: (a) Current density showing a triplicate experiment by re-using the same electrode, and (b) the corresponding product yields during the electrochemical reduction of oxalic acid for 2 h at an optimal potential of −0.6 V vs RHE at a temperature of 25 °C.

Bulk electrolysis for 12 h

A potential of −0.6 V *vs* RHE was applied in long-term oxalic acid conversion. The current density, percentage conversion of oxalic acid, and product yields are depicted in Figure S4. A 91% conversion of the oxalic acid was achieved (Figure S4b, red line). Evaluation of the product yields showed that glyoxylic acid was the major product in the early hours of the experiment (Figure S4b, green line). However, the concentration of the glyoxylic acid tended to decrease after 6 h of the experiment, while that of glycolic acid increased, with glycolic acid being the major product towards the end of the experiment (Figure S4b, blue line). This is because some of the glyoxylic acid produced is converted to glycolic acid, thereby decreasing its concentration. A similar trend was observed even at a lower applied potential of −0.5 V RHE, albeit with an overall lesser percentage conversion of oxalic acid and product yield, as illustrated in Figure S5.

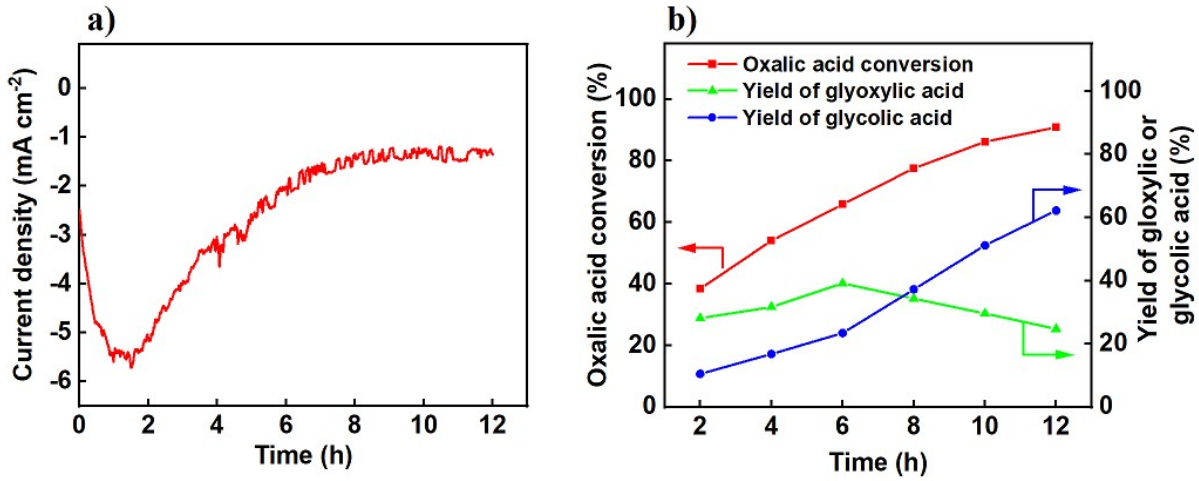

Figure S4: (a) Current density showing a long-term oxalic acid conversion at −0.6 V *vs* RHE, and (b) conversion profiles of oxalic acid and product yields during electrochemical reduction for 12 h at an applied potential of −0.6 V vs RHE at a temperature of 25 °C.

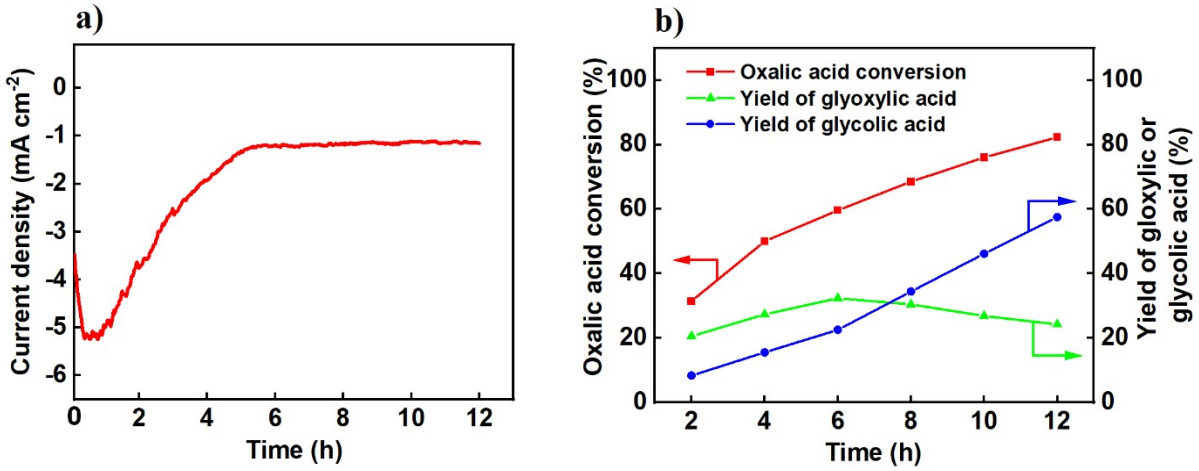

Figure S5: (a) Current density showing a long-term oxalic acid conversion at −0.5 V *vs* RHE, and (b) conversion profiles of oxalic acid and product yields during electrochemical reduction for 12 h at an applied potential of −0.5 V vs RHE at a temperature of 25 °C.

Cyclic Voltammetry

Cyclic voltammetry measurements were conducted using a Gamry potentiostat/galvanostat (Gamry Instruments Interface 1010E) in a conventional three-electrode glass cell. The working electrode was titanium foil, having a surface area of 2 cm^2, while the counter electrode was a platinum foil of the same dimensions as the working electrodes, and a saturated calomel electrode (SCE) served as the reference electrode. Similarly, to evaluate the changes that may occur on the electrode during electrolysis, another cyclic voltammetry measurement was performed after bulk electrolysis; the outcomes are represented in Figure S6. From the voltammograms, only modest changes were observed on the electrode. All potentials were measured relative to SCE. All potentials measured against SCE were then converted to RHE using the relation ($E_{RHE} = E_{SCE} + 0.244\ V + 0.059 \times pH$). The same was done for potentials measured against Ag/AgCl ($E_{RHE} = E_{Ag/AgCl} + 0.1976\ V + 0.059 \times pH$)[2] to enable comparison with the outcomes reported by other researchers. Cyclic voltammetry experiments were conducted at 25 °C.

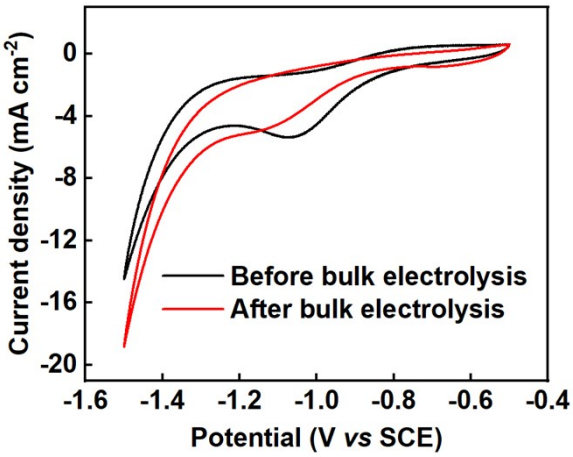

Figure S6: Cyclic voltammetry of a titanium electrode with a surface area of 2 cm^2 in 0.03 M oxalic acid in 0.2 M Na_2SO_4 (a) before bulk electrolysis (black line) and (b) after bulk electrolysis at an optimal potential of −0.6 V vs RHE for 12 hours (red line). The measurements were taken at a scan rate of 50 mV s^{-1} and a temperature of 25 °C.

X-ray Diffraction (XRD) Analysis

Figure S7 shows the X-ray diffraction (XRD) pattern of the titanium electrode before and after electrolysis to understand its crystalline structure in detail. Generally, the titanium oxides consist of sub-oxide forms having the general formula Ti_nO_{2n-1} where $3 < n < 10$ (such as TiO_2, Ti_2O, Ti_3O_5, Ti_4O_7, Ti_5O_9, Ti_6O_{11}, etc.).[5] These oxides display different properties, such as high electrical conductivity and chemical stability. The electrical conductivity values vary depending on the sub-oxide ('n' value) structure.[5]

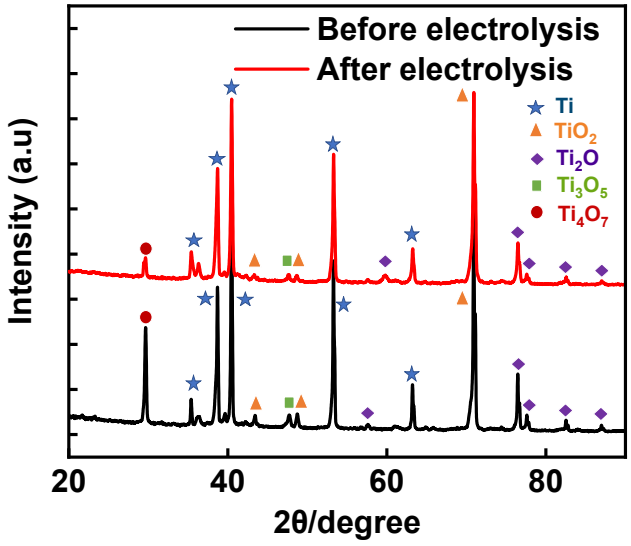

Figure S7: XRD spectra of a titanium electrode before (black line) and after electrolysis (red line) at an applied potential of −0.6 V vs RHE for 2 hours at 25 °C.

X-ray Photoelectron Spectroscopy (XPS) Analysis

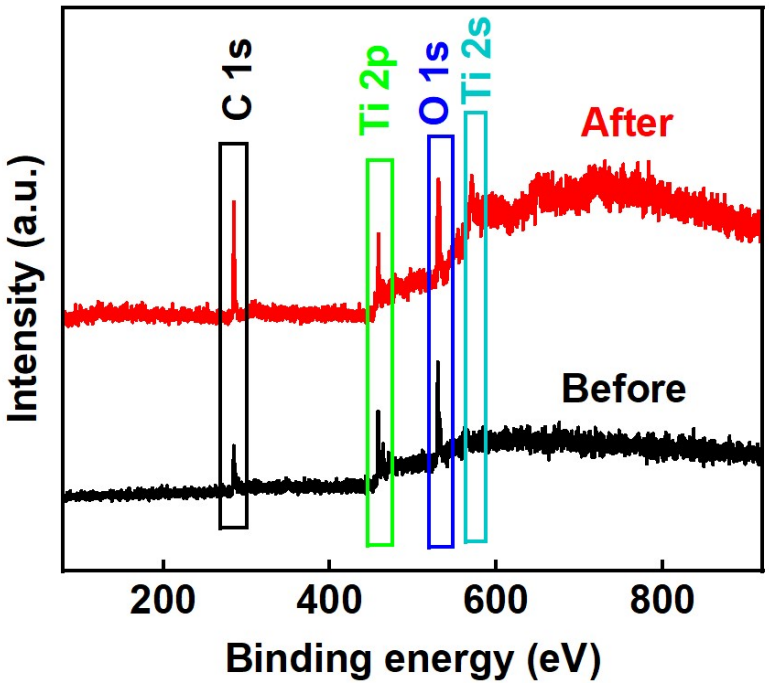

Figure S8: XPS survey spectra of a titanium electrode before (black line) and after electrolysis (red line) at an applied potential of −0.6 V vs RHE for 2 hours at 25 °C.

Ellipsometry

Ellipsometry was performed to determine the thickness of the native oxides.[6] Ellipsometry was achieved using a variable-angle ellipsometer (M-2000XI Ellipsometer, J. A. Woollam) to measure the amplitude and phase changes in the wavelength range 210-1690 nm at angles of incidence 45°, 50°, 55°, 60°, 65°and 70°. This was done at 9 different positions on the sample before and after electrolysis. The ellipsometry data was fitted with a Ti substrate (Lorentz) and the native oxide was fitted with a B-Spline, from which the thickness was extracted from the fitting. A fitting model for one of the positions on the sample compared to experimental psi and delta at different angles before and after electrolysis is shown in Figure S9. The ellipsometry data suggest a decrease in the thickness of the native oxide after electrolysis, as shown in Table S2. The reduction in the thickness of the native oxides of titanium after electrolysis could be due to the etching of the oxides by the acid,[7,8] or else to the reduction of part of the oxide to the metal during electrolysis.

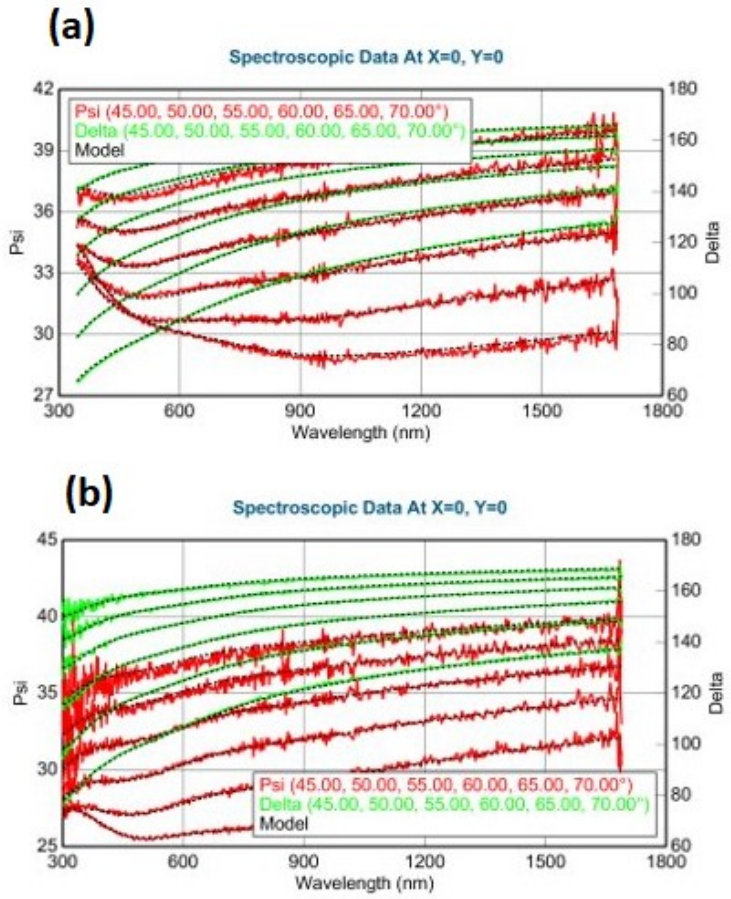

Figure S9: The ellipsometry fitting model (black) and experimentally measured Ψ (psi) and Δ (delta) (red and green, respectively) at different angles for the titanium electrode (a) before and (b) after electrolysis.

Table S2: The average thickness of the native oxides of Ti obtained from the ellipsometry data across all the angles analysed.

Electrode	Thickness of the native oxides (nm)
Before electrolysis	48.4 ± 0.4
After electrolysis	17.9 ± 1.5

Atomic Force Microscopy (AFM)

Atomic Force Microscopy (AFM) analysis was performed to evaluate the roughness/smoothness of the native oxides. Table S3 presents the roughness value of the electrode surface before and after electrolysis.

Table S3: Atomic force microscopy data showing the roughness value of the electrode surface before and after electrolysis.

Electrode	Average height of the peak, S_h (nm)	Average roughness, R_a (nm)	Root mean square roughness, R_q (nm)
Before electrolysis	143	26.2	35.2
After electrolysis	317	38.3	49.7

Electrochemically Active Surface Area (ECSA)

First, a non-Faradaic potential range was identified from the titanium electrode's cyclic voltammogram. Over the region, −0.05 to −0.40 V, depicted in Figure S10(a), a series of cyclic voltammetry scans were performed at different scan rates (10, 50, 100, 200, 300, 400, 600, 800, 1000 mV s^{-1}). The electrode's electrochemically active surface area (ECSA) was calculated using Equation S5.

$$ECSA = \frac{C_{DL}}{C_S} \qquad (Equation\ S5)$$

Where C_{DL} = Double-layer capacitance and C_S = Specific capacitance.

To measure the electrode's capacitance, it is assumed that all the measured current in the non-Faradaic region is due to the double-layer charging of Ti/Ti_xO_y.[4] Based on this assumption, the charging current (i_c) is measured from the cyclic voltammograms of the multiple scan rates in Figure S10a. The current obtained is equal to the product of the electrochemical double-layer capacitance (C_{DL}) and the scan rate (v), as shown in Equation S6

$$i_c = vC_{DL} \qquad (Equation\ S6)$$

A plot of i_c against v gives a straight-line graph with a slope equal to C_{DL} (Figure S10b).

Thus, the electrochemical double-layer capacitance of the electrode, C_{DL} = 0.18 × 10^{-3} A·s V^{-1} (0.18 mF).

Thus, the specific capacitance (C_S) values can be calculated from the cyclic voltammograms by using Equation S7[9]

$$C_S = \frac{1}{\Gamma v\,(V_2 - V_1)} \int_{V_1}^{V_2} I(V)\,dV \qquad \text{(Equation S7)}$$

Where $\boldsymbol{\Gamma}$ is the area of the working electrode in cm^2, v is the scan rate in V s^{-1} and ($V_2 - V_1$) is the potential window expressed in V. The specific capacitance at a scan rate of 1 V s^{-1} was found to be 1.21 × 10^{-4} A·s V^{-1} cm^{-2}. By substituting the values of capacitance and the specific capacitance into equation 5, an ECSA value of 1.49 cm^{-2} was obtained. This ECSA value can be compared with other electrode materials like Ni (0.43 cm^{-2}), Au (1.7 cm^{-2}), and Mn (3.2 cm^{-2}).[10–12] Hence, the electrodes' ESCAs can be arranged in the order Mn > Au > Ti > Ni.

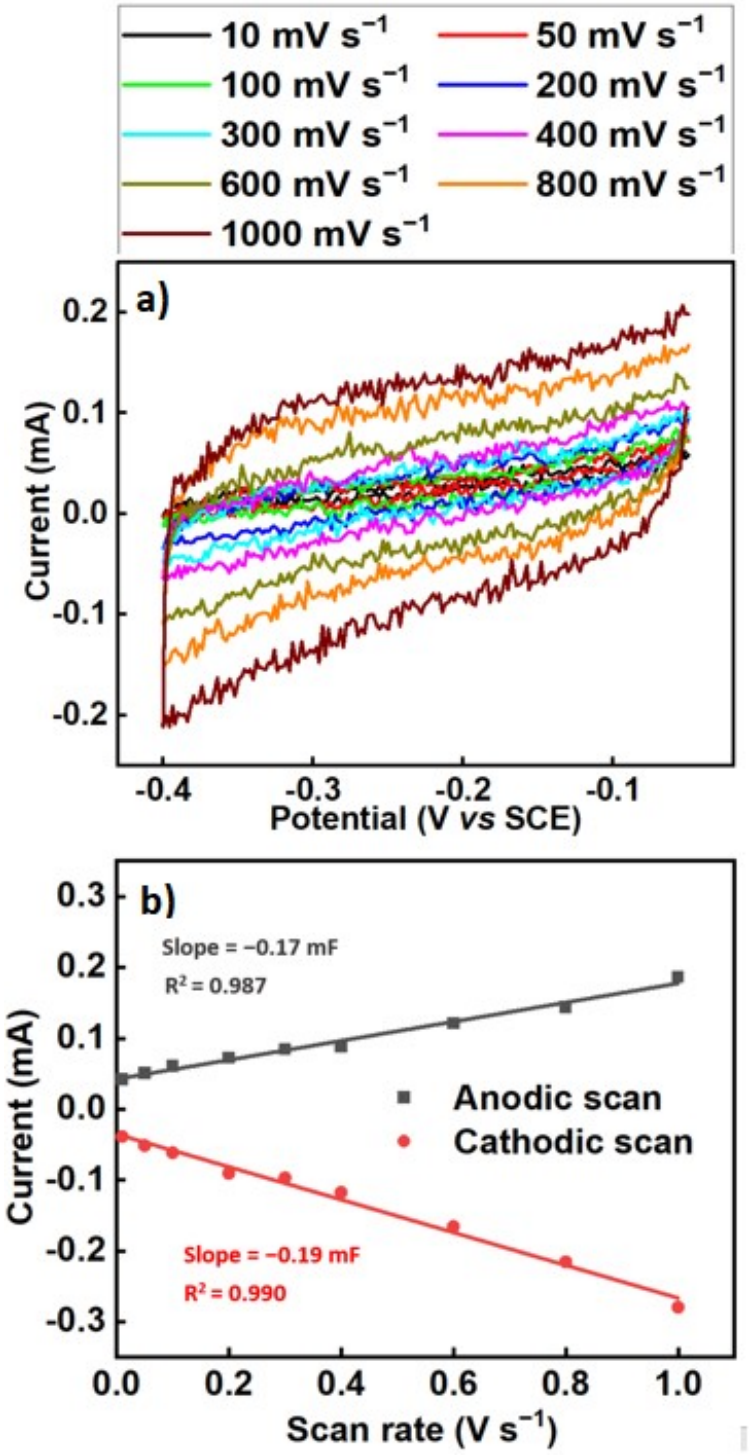

Figure S10: Double-layer capacitance measurements for determining the electrochemically active surface area of a titanium electrode (Ti/Ti_xO_y) in oxalic acid solution and 0.2 M tetraethyl ammonium chloride as supporting electrolyte. (a) Cyclic voltammograms of the non-Faradaic region at different scan rates using platinum foil as a counter electrode and SCE as a reference electrode. (b) The anodic (black cubes) and cathodic (red circles) charging currents measured at −0.23 V vs SCE were plotted against the scan rate. The determined double-layer capacitance of the electrode is taken as the average of the absolute values of the slopes of the linear fits of the data.

Electrochemical Impedance Spectroscopy (EIS)

The electrical equivalent circuit model that describes the electrode processes was determined by fitting the experimental impedance data using Gamry Echem Analyst software. Various equivalent circuit models were examined to describe the electrode processes at the Ti/Ti_xO_y /electrolyte junction. The simplest circuit with the smallest chi-square (χ^2) value was chosen and applied according to the methods developed in the literature.[13–16] The electrical parameters of the proposed equivalent circuits obtained after fitting the results of the EIS tests for the titanium electrodes are presented in Table S4. In the equivalent circuit model, R_s refers to the solution resistance, while R_1 and R_2 represent charge transfer resistance. CPE_1 and CPE_2, representing the constant phase elements, are commonly used to describe nonhomogeneous surfaces.[17] In addition to this, the total resistance of the layer (R_{total}), representing the sum of all resistance values, is also calculated (Table S4). The R_{total} value for the titanium electrode prior to electrolysis is 88.32 Ω, whereas it decreases to 59.21 Ω after electrolysis. This decrease is consistent with an increase in the electroactive area when a potential is applied, leading to improved electron transfer through the conductive layers. The observed reduction in R_{total} is consistent with a decrease in the thickness of the titanium oxide layer after electrolysis. The alterations in film thicknesses and total resistances suggest notable changes in the composition and morphology of the electrode surfaces.

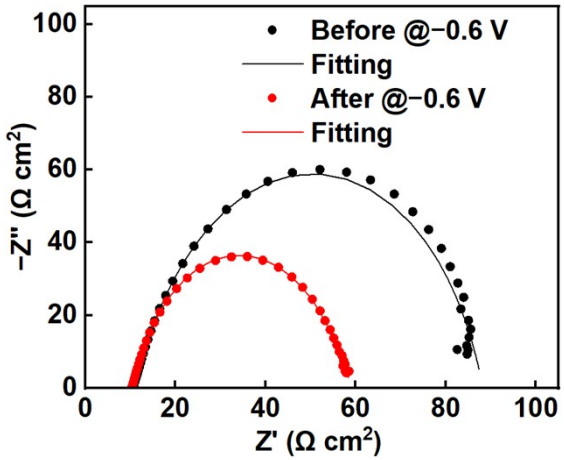

Figure S11: Nyquist plots obtained at −0.6 V vs RHE on a titanium electrode in 0.03 M oxalic acid solution (a) before electrolysis and (b) after electrolysis for 2 hours at 25 °C. Cycle points represent the experimental data, and continuous curves represent the model fitting.

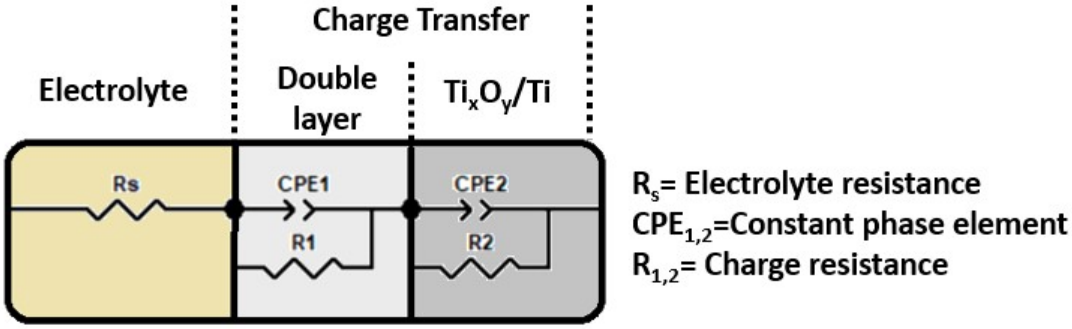

Figure S12: Electrical equivalent circuit model of a titanium electrode.

Table S4: Electrical parameters of the proposed equivalent circuits obtained after fitting the results of EIS tests for titanium electrodes.

Electrodes	R_s/ Ω	R_1/ Ω	CPE_1 mF	n_1	R_2/ Ω	CPE_2 mF	n_2	R_{total}	Chi-squared χ^2
Before	10.52	12.9	6.05	0.60	64.9	7.51	0.86	88.32	2.22×10^{-4}
After	10.29	13.01	8.98	0.59	35.91	7.60	0.89	59.21	1.77×10^{-5}

References

1 F. P. Abramo, F. De Luca, R. Passalacqua, G. Centi, G. Giorgianni, S. Perathoner and S. Abate, *J. Energy Chem.*, 2022, **68**, 669–678.

2 L. Fan, C. Xia, P. Zhu, Y. Lu and H. Wang, *Nat. Commun.*, 2020, **11**, 1–9.

3 C. C. L. McCrory, S. Jung, J. C. Peters and T. F. Jaramillo, *J. Am. Chem. Soc.*, 2013, **135**, 16977–16987.

4 C. C. L. McCrory, S. Jung, I. M. Ferrer, S. M. Chatman, J. C. Peters and T. F. Jaramillo, *J. Am. Chem. Soc.*, 2015, **137**, 4347–4357.

5 Z. Ertekin, U. Tamer, K. Pekmez, *Electrochimica Acta*, 2015, **163**, 77–81.

6 W. Navarrini, T. Brivio, D. Capobianco, M. V. Diamanti, M. Pedeferri, L. Magagnin and G. Resnati, *J. Coatings Technol. Res.*, 2011, **8**, 153–160.

7 J. Winiarski, A. Niciejewska, M. Górnik, J. Jakubowski, W. Tylus and B. Szczygieł, *RSC Adv.*, 2021, **11**, 21104–21115.

8 P. Vlcak, J. Fojt, J. Drahokoupil, V. Brezina, J. Sepitka, T. Horazdovsky, J. Miksovsky, F. Cerny, M. Lebeda and M. Haubner, *Mater. Sci. Eng. C*, 2020, **115**, 111065.

9 K. M. Thulasi, S. T. Manikkoth, A. Paravannoor, S. Palantavida and B. K. Vijayan,

International Journal of Materials Science, 2021, **112**, 937–944.

10 E. Cossar, M. S. E. Houache, Z. Zhang and E. A. Baranova, *J. Electroanal. Chem.*, 2020, **870**, 114246.

11 S. Zhao, H. Yu, R. Maric, N. Danilovic, C. B. Capuano, K. E. Ayers and W. E. Mustain, *J. Electrochem. Soc.*, 2015, **162**, F1292–F1298.

12 P. Connor, J. Schuch, B. Kaiser and W. Jaegermann, *Zeitschrift fur Phys. Chemie*, 2020, **234**, 979–994.

13 S. Popescu, C. Ungureanu, A. Albu, C. Pirvu, *Progress in Organic Coatings,* (2014), **77**, 1890–1900.

14 M. R. Jakeria, R. J. Toh, X. B. Chen and I. S. Cole, *J. Appl. Electrochem.*, 2022, **52**, 1021–1044.

15 A. Faqeeh, M. D. Symes, *Electrochimica Acta*, **444**, (2023) 142030.

16 M. Ghadirzadeh, K. Jafarzadeh, H. M. Abassi, S. M. Mirali, *Materials Chemistry and Physics,* 2024, **314,** 128782.

17 A. C. Alves, F. Wenger, P. Ponthiaux, J. P. Celis, A. M. Pinto, L. A. Rocha and J. C. S. Fernandes, *Electrochim. Acta*, 2017, **234**, 16–27.